A Comprehensive Flood Inundation Mapping for Hurricane Harvey Using an Integrated Hydrological and Hydraulic Model

MENGYE CHEN,[a,b] ZHI LI,[a,b] SHANG GAO,[b] XIANGYU LUO,[b] OLIVER E. J. WING,[c,d] XINYI SHEN,[e] JONATHAN J. GOURLEY,[f] RANDALL L. KOLAR,[a] AND YANG HONG,[a,b]

[a] *School of Civil Engineering and Environmental Sciences, University of Oklahoma, Norman, Oklahoma*
[b] *Hydrometeorology and Remote Sensing Laboratory, University of Oklahoma, Norman, Oklahoma*
[c] *Fathom, Bristol, United Kingdom*
[d] *School of Geographical Sciences, University of Bristol, Bristol, United Kingdom*
[e] *Department of Civil and Environmental Engineering, University of Connecticut, Storrs, Connecticut*
[f] *NOAA/National Severe Storm Laboratory, Norman, Oklahoma*

(Manuscript received 18 September 2020, in final form 29 March 2021)

ABSTRACT: Because climate change will increase the frequency and intensity of precipitation extremes and coastal flooding, there is a clear need for an integrated hydrology and hydraulic system that has the ability to model the hydrologic conditions over a long period and the flow dynamic representations of when and where the extreme hydrometeorological events occur. This system coupling provides comprehensive information (flood wave, inundation extents, and depths) about coastal flood events for emergency management and risk minimization. This study provides an integrated hydrologic and hydraulic coupled modeling system that is based on the Coupled Routing and Excessive Storage (CREST) model and the Australia National University-Geophysics Australia (ANUGA) model to simulate flood. Forced by the near-real-time Multi-Radar Multi-Sensor (MRMS) quantitative precipitation estimates, this integrated modeling system was applied during the 2017 Hurricane Harvey event to simulate the streamflow, the flood extent, and the inundation depth. The results were compared with postevent high-water-mark survey data and its interpolated flood extent by the U.S. Geological Survey and the Federal Emergency Management Agency flood insurance claims, as well as a satellite-based flood map, the National Water Model (NWM), and the Fathom (LISFLOOD-FP) model simulated flood map. The proposed hydrologic and hydraulic model simulation indicated that it could capture 87% of all flood insurance claims within the study area, and the overall error of water depth was 0.91 m, which is comparable to the mainstream operational flood models (NWM and Fathom).

SIGNIFICANCE STATEMENT: We wanted to provide a tool for local emergency response officials to visualize the possible flood conditions in their region, because the heavy rainfall flood is likely becoming more frequent and more intense, possibly as a result of climate change. The simulated flood information includes the water channel flowrate, two-dimensional flood extent, and the inundation depth throughout the flooded area. The results proved that, with less data requirement, the proposed tool can provide the comprehensive flood information, with accuracy of flood extent simulation comparable to mainstream flood models and acceptable inundation-depth simulation. We will keep working to expand the capability of the framework from the real-time simulation to the 1-h lead-time prediction.

KEYWORDS: North America; Hurricanes; Coupled models; Hydrologic models; Model comparison; Model evaluation/performance

1. Introduction

Flooding triggered by excessive precipitation is the second-deadliest and most common natural hazard in the United States and worldwide (Ashley and Ashley 2008; Barredo 2007; Benito et al. 2004; Smith and Ward 1998), which accounts for 43% of total natural disasters from 1995 to 2015 recorded by the United Nations (Wallemacq et al. 2015). The Gulf Coast and the South Atlantic Coast of the United States are profoundly affected by extreme precipitation from tropical cyclones and their resulting floods (Adhikari et al. 2010), which is responsible for around 25 000 fatalities in the United States since 1942 (Rappaport 2000, 2014). For pluvial floods, the precipitation rate, duration, the land use of the region, topography, and antecedent soil moisture conditions are the main factors to determine the overall flood severity (Brauer et al. 2020). Recent studies indicate that the frequency and intensity of extreme rainfall and tropical cyclones will likely increase (van Oldenborgh et al. 2018) and the propagation of the cyclones will likely decrease due to the possible impact from climate change (Kossin 2018). It is thus likely that the future flood risk and its consequential socioeconomic damage will escalate. On top of the changes in the tropical cyclone characteristics, rising sea level in a warming climate can intensify coastal flooding (Wing et al. 2019). There is a clear need for tools that can facilitate the current and future flood risk mitigation.

One of those tools is an improved, real-time flood prediction system, which supports multidisciplinary decision making including but not limited to: first-responder preparedness,

Denotes content that is immediately available upon publication as open access.

Corresponding author: Mengye Chen, mchen15@ou.edu

DOI: 10.1175/JHM-D-20-0218.1

temporary flood defense planning, insurance budgeting, and supply chain management. Flood prediction and inundation mapping have been studied for over a century, and two traditional groups of research efforts have gained most of the attention of the research community: observations and hydraulic models (Teng et al. 2017). The observation methods include ground measurements, surveys, and remote sensing technology (Shen et al. 2019b,a; Syvitski and Brakenridge 2013). As remote sensing technologies can identify the flood extent over a vast area, while other observation methods can only provide data at single points, flood mapping aided by remote sensing has gained popularity in recent years. However, because of limitations such as data latency, the observation-based results are more often used as an input or as a benchmark to validate and calibrate hydrological and hydraulic models (Teng et al. 2017).

Hydraulic models include one-dimensional, two-dimensional, and three-dimensional methods that use the physical equations and laws to describe fluid motion where the degree of complexity varies. The one-dimensional hydraulic model is considered the most straightforward representation of floodplain flow, as it simulates the open surface water flow with the assumption that the water only flows in one direction. The flow velocity is then averaged over the channel cross section (Brunner 2016). The 2D model assume the water as a shallow ditch, and no flow occurs vertically, and then the shallow-water equation is solved from the depth-averaged Navier–Stokes equations (Roberts et al. 2019). In some individual cases which need detailed information for engineering solutions, such as dam breaks, tsunamis, or embankment failures, 3D hydraulic models are implemented. However, for most of the floodplain analysis and simulation, the 2D shallow-water approximation is considered adequate after proper model construction and validation (Alcrudo 2004). The fully solved the 2D St. Venant shallow-water equations using the finite-volume and finite-element methods are considered to have a higher complexity among the 2D hydraulic models (Bates and De Roo 2000). The storage cell or the cellular automata approach by solving Manning's equation with finite-difference methods, such as the ''LISFLOOD-FP'' model, was suggested to be a good approximation to the physics-based model and the computation time was reduced by 30 times (Ghimire et al. 2013). It was further tested to prove the method was as efficient as other classes of models implementing HPC techniques (Bates et al. 2010).

Integrating hydrologic model and hydraulic models has the benefit of utilizing present-day computational resources to model dynamic representations of extreme hydrometeorological events (Anselmo et al. 1996). A recent study (Tanaka et al. 2018) has integrated three difference models: a distributed hydrological model called Geomorphology-Based Hydrological Model (GBHM), a 1D hydraulic model named Mike11, and a 2D hydraulic model called Local Inertial Equation (LIE). The study found the integrated framework yielded good agreement between with the observation data of the stream discharge, as well as the lake water level over a 4-yr span. It was able to simulate a significant flooding event in 2000 over the study area. The authors also indicated that the framework could simulate sediment movement downstream in the future research plan.

Since 2016, the Ensemble Framework For Flash Flood Forecasting (EF5) integrated the Coupled Routing and Excess Storage (CREST) distributed hydrological model, a 1D hydraulic model, with kinematic wave channel routing, to successfully simulate multiple extreme precipitation-triggered flash flooding events in Oklahoma City and Houston at a continental-scale implementation (Flamig et al. 2020; Gourley et al. 2017). Outside the United States, the CREST was coupled with an 1D fully distributed linear reservoir routing scheme and found success over a study in China (Shen et al. 2017). The National Water Center led an effort to integrate the WRF-Hydro hydrologic model and the Height Above Nearest Datum (HAND) inundation mapping method into the new National Water Model (NWM; Cohen et al. 2018). The HAND method performed a simulation of a 2016 Texas flooding event with good agreement with remote sensing observations and less computation cost (Zhang et al. 2018). A recent study by (Wing et al. 2019), compared the flood-mapping performances for Hurricane Harvey between NWM+HAND and Fathom, a LISFLOOD-FP-based hydraulic modeling system that contains all major hydrological and hydraulic components to describe the water dynamics. The study results indicated that Fathom outperformed NWM+HAND according to all statistical metrics and could better capture the pluvial and coastal flooding phenomena. The public would greatly benefit from a comprehensive and accurate flood extent and inundation-depth predictions for tropical cyclone events to improve local risk management.

A ''grand challenge for hydrology'' was raised by (Wood et al. 2011) to provide hyper-resolution hydrological prediction capacities to the public, as the society critically demands the high spatial–temporal resolution forecasting for floods and droughts. New remote sensing technology provides accurate and high spatially and temporally resolved observations over the globe, which helps to advance physics-based models for atmospheric, hydrologic and hydraulic forecasting. However, the remote sensing products are not error-free and these errors in precipitation products can be further propagated to the hydrologic and hydraulic modeling results (Hong et al. 2006); therefore, the accuracy of the input precipitation data is crucial for flood applications. The Multi-Radar Multi-Sensor system (MRMS), which utilizes data from over 180 NEXRAD radars and covers the conterminous United States at 1-km spatial resolution with a 2-min update frequency (Zhang et al. 2016), has shown more accuracy during Hurricane Harvey event than did NASA's Integrated Multisatellite Retrievals for GPM (IMERG) v6 product and National Centers for Environmental Prediction (NCEP) gridded gauge only precipitation production; and has good agreement with the Harris County Flood Control District (HCFCD) rain gauge data (Chen et al. 2020; Li et al. 2020). This study, again, uses Hurricane Harvey as the study case, since it was considered a 100–500-yr flood event, which caused the local streams' return period reduced 20%–35% after the event (Vu and Mishra 2019; McDonald and Naughton 2019).

The overarching goal of the study is to first introduce the newly developed hydrology and hydraulic model CREST-inundation

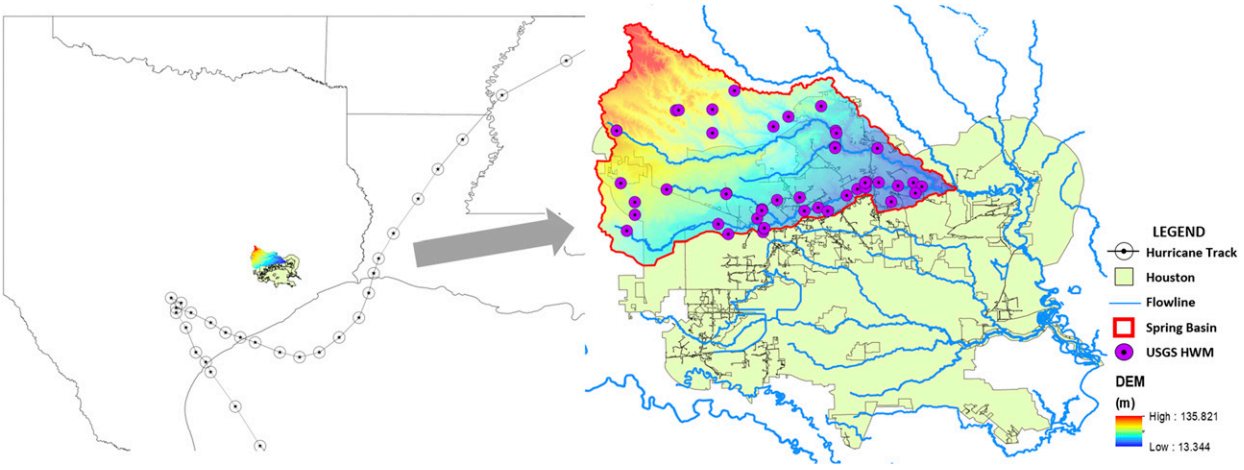

FIG. 1. Study area showing Hurricane Harvey storm track, City of Houston Spring basin and its topography, and HWM locations.

Mapping and Prediction (CREST-iMAP) as a latest addition of the well-documented CREST hydrologic modeling family; and to further test and compare this new coupled system with some other the-state-of-the-art flood-mapping models in an extreme storm event setting. Additionally, the physics-based 2D hydrological-hydraulic CREST-iMAP model provides ease on scale-up implementation with less data preparation requirement and streamflow-only calibration processes. More specified objectives of this study are to 1) design and develop the CREST-iMAP which couples the hydrologic and hydraulic components, while bypassing the river channel data requirement; 2) evaluate the flood extent by comparing the modeling results with the observed U.S. Geological Survey (USGS) flood map, satellite-based (SAR) flood map, Fathom flood map, NWM+HAND flood map, and the Federal Emergency Management Agency (FEMA) flood insurance claims map for Hurricane Harvey, and 3) evaluate the flood inundation depths between the USGS high-water marks (HWMs), Fathom flood map, NWM+HAND flood map, and CREST-iMAP simulated flood map using statistic methods. This paper is organized as follows. Section 2 describes the study area, data, the description of the CREST hydrologic model and 1D hydraulic model, Fathom, and the evaluation methods. Section 3 discusses the results of the intercomparison of the flood maps from the USGS interpolation, SAR data, the Fathom simulation, the NWM+HAND simulation, and the CREST-iMAP-based simulation. Section 4 concludes the study and proposes future directions.

2. Methods and data

a. Study area and data

Hurricane Harvey made the first landfall on northern San Jose Island, Texas, on 26 August 2017, and moved along the Texas Coast for almost 5 days before the second landfall on 30 August 2017 (Blake and Zelinsky 2018). Hurricane Harvey poured over 1500 mm of water on the Great Houston area (Brauer et al. 2020). Figure 1 displays the Hurricane track, the boundary of Houston, the Spring basin, major flowlines, and the USGS HWMs within the Spring basin. The Spring basin, located in the northwestern part of the Great Houston area, was selected for this study. The Spring basin is among the most impacted areas during Hurricane Harvey (National Weather Service 2018). It has mixed land-cover types across the basin (Chen et al. 2020), which was believed to be an underperforming area by another study (Wing et al. 2019). There are four major rivers within the Spring basin: Spring Creek, Willow Creek, Little Cypress Creek, and Cypress Creek, entering Lake Houston and 55 USGS HWM sites measured for the Hurricane Harvey event. The HWM sites are more concentrated along Cypress Creek and the southeastern part of the basin because the area has more urban development.

The MRMS radar-based quantitative precipitation estimates (QPE) were obtained from the Iowa Environmental Mesonet NWS data archive (https://mesonet.agron.iastate.edu/nws/). The 15-min streamflow data of five stream gauges across the basin from 1 April to 3 September 2017 were obtained from the USGS National Water Information System (https://waterdata.usgs.gov/nwis). The hyper-resolution (10 m) digital elevation model (DEM) was obtained from USGS Earth Explorer (https://earthexplorer.usgs.gov/). The 250-m-resolution hydrologically conditioned DEM was obtained from HydroSHEDS (https://www.hydrosheds.org/; Lehner et al. 2008). The 10-m-resolution CREST parameters were derived and calculated using methods described in Vergara et al. (2016) from the USGS Soil Survey Geographic Database (SSURGO). The 1-km-resolution CREST parameters were passed from the beginning phase of the Flooded Locations and Simulated Hydrographs (FLASH) project to input to the hydrological modeling portion of the CREST-iMAP. The U.S. land-cover data were obtained from Multi-Resolution Land Characteristics Consortium (MRLC; https://www.mrlc.gov/), and it was extended to arrive at gridded Manning's roughness coefficients as described in (Liu et al. 2019). The USGS HWM data and FEMA property claim data during Hurricane Harvey were obtained from HydroShare (https://hydroshare.org; Arctur et al. 2018). The USGS daily potential evapotranspiration (PET) data were obtained from

USGS Famine Early Warning Systems Network (FEWS NET; https://earlywarning.usgs.gov/fews).

b. CREST inundation mapping and prediction (CREST-iMAP) framework

CREST is a grid-based, distributed hydrological model that was developed by the University of Oklahoma and NASA Applied Science Team (Wang et al. 2011). The EF5 framework later included CREST as one of the water balance modeling cores and coupled it with the kinematic wave channel routing method, and the framework can provide hydrological simulation at continental and global scales (Clark et al. 2017). Researchers have adapted the EF5 framework for high-resolution flash flood forecasting in the United States (Flamig et al. 2020). It now serves as the backbone of FLASH, which was transitioned to the NWS in November 2016 and has evolved the tools for operational flash flood forecasting (Gourley et al. 2017). The NWS Weather Forecast Offices (WFOs) have reported that having FLASH data were extremely useful by allowing staff to focus in on threats and upgrade warnings more rapidly and timely (National Weather Service 2018). This study uses a modified EF5 framework from the implemented version in the FLASH project, which is used as water balance component of the CREST-iMAP. CREST is coupled with the Australia National University and Geoscience of Australia (ANUGA) hydraulic model (Nielson et al. 2005). The ANUGA model was built on the basis of a finite-volume method for solving the 2D shallow-water equation (Roberts et al. 2019), to simulate the floodplain flow movement and assume that water depth is much less than the water movements in x and y directions (Teng et al. 2017). However, the ANUGA model only simulates the 2D water-depth distribution and flow velocity, while the water–soil and water–atmosphere interactions are not considered in the modeling framework. Therefore, an additional component of water balancing is needed to meet that need.

In this study, the EF5-CREST model was one-way and offline coupled with the ANUGA model to comprehensively provide flood information, including streamflow, flood extent, and inundation depth. Figure 2 illustrates the schematic flowchart of CREST-iMAP coupling mechanics. CREST-iMAP receives forcing precipitation data, such as radar/satellite QPE, machine-learning modeled or numerically modeled quantitative precipitation forecasts (QPF), or an interpolated rainfall field. The hydrological model simulates and generates excessive rainfall, soil moisture, and streamflow, where excessive rainfall as well as soil moisture are further used to drive and set the initial soil condition for the hydraulic model (ANUGA), and the streamflow is the one-dimensional output from the CREST-iMAP. The water balance module has 17 parameters to describe the physical interactions among water, soil, and air (Wang et al. 2011), whereas the hydraulic model has only the Manning's roughness coefficient that governs the water flow (Roberts et al. 2019). The simulated streamflow is the variable used to calibrate the model parameters based on comparisons with USGS stream gauge records. The hydraulic model receives the excessive rainfall data field from each time step and simulates two variables in a single raster file to illustrate the flood extent and the flood inundation depth to the end user.

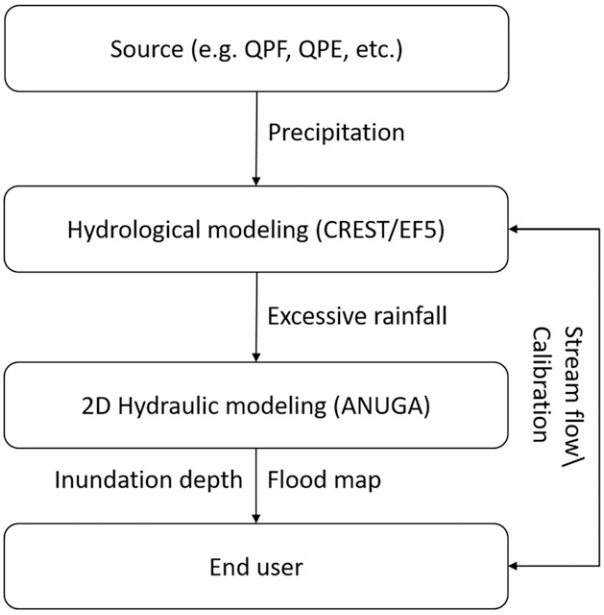

FIG. 2. The schematic data flowchart of CREST-iMAP. One component (specified in the boxes) becomes the input of another, and arrows represent the data flow.

The CREST-iMAP has a few key sciences that are embedded in this model. First, the canopy interception is simulated using the Canopy Interception Capacity method (Dickinson et al. 1989), which is derived from the land-cover data. The infiltration process is simulated using the University of Washington Variable Infiltration Curve (VIC; Liang et al. 1996a,b) model. The evapotranspiration and soil-drying process is simulated by a decision-tree process described in Wang et al. (2011), which is driven by the PET data. The subsurface water routing is done in the one-dimensional fashion using the 1D kinematic wave method to feedback to channel streamflow (Lighthill and Whitham 1955), and not involved in 2D water routing. Only the excessive rainfall is left on the surface for 2D water routing simulated by the St. Venant equation to produce the overland flood. The sciences support the application of CREST-iMAP to simulate the precipitation-triggered flood events, when ET is not the major contributing factor. Since the finite-volume-method hydraulic model has high robustness (Horritt and Bates 2002), the CREST-iMAP can bypass the river channel data requirement and only the water balance parameters are designed to be calibrated.

In this study, the MRMS near-real-time QPE was input to CREST-iMAP at 2-min temporal resolution. To imitate the nested real-time operational scheme, the water balance module calculates the excessive rainfall at 250-m resolution and simulated streamflow on all water channels using 250-m DEM and 1-km parameters, which were calibrated with five USGS stream gauges described in (Chen et al. 2020), using DREAM methods (Vrugt 2016; Vrugt et al. 2009). The calibrated excessive rainfall was then read by a hydraulic module at 2-min

temporal resolution, and the internal calculation time step is 10 s on an approximately 10 by 10 m^2 area triangular mesh. At each steps of the coupled modeling, the calculation is done at the optimal temporal–spatial resolutions for the stability and efficiency purposes of each module, which are 250 m and 15 min for the water balance, as well as 10 m and 10 s for hydraulic routing. Therefore, the 1-km-resolution MRMS QPE is first calculated into 250-m excessive rainfall field and then is calculated to water depth and water fluxes at 10-m resolution. The model output was extracted every 15 min and further interpolated to the 10-m-resolution raster files. For more accurate simulation of the flooding impact of Hurricane Harvey, the water balance module utilized a warmup period from 1 April to 25 August 2017 and coupled the simulation period from 25 August to 3 September 2017. This approach is an attempt to use the native DEM with no manipulation and bypass the detailed river channel information, which is not available at all locations and problematic for an operational flood prediction system (Orzech et al. 2011; Lejot et al. 2007; Merwade et al. 2006). All flow direction and flow accumulation data were derived from the original DEM and relied on its quality. Therefore, CREST-iMAP can reduce the data requirement for model applications relative to traditional 2D hydraulic modeling (Brunner 2016). CREST-iMAP is designed to operate in the real time and provide timely flood information; therefore, the group of flood maps used in the comparison is from real-time operational systems around the world.

c. *Fathom model (LISFLOOD-FP)*

Fathom-Global is a framework that combines multiple continental-scale hydraulic model implementations (Wing et al. 2017), among which was first described by (Sampson et al. 2015). Fathom utilizes the LISFLOOD-FP as the computational core, which solves the local inertial form of the shallow-water equations using a 2D regular grid (de Almeida and Bates 2013; Bates et al. 2010; Bates and De Roo 2000). In this study, the Fathom-simulated flood map was generated using the river discharge data as the forcing, which was the USGS stream gauge observations at the related inflow points in the stream network (Wing et al. 2019). The pluvial flood was also considered by inputting the U.S. Weather Prediction Center stage-IV rainfall data onto the grid cells. The infiltration was considered using a simplified infiltration capacity method, using the information from the Harmonized World Soil Database derived by a modified Hortonian infiltration equation (Morin and Benyamini 1977). The simulation also included levee information, burned-in channels, and storm-surge simulation to capture the multiple phenomena contributing to the Hurricane Harvey flood at 10-m spatial resolution. These data are from an operational Fathom–U.S. version, which was built upon and updated from a high-resolution global flood hazard model (Wing et al. 2019; Sampson et al. 2015), which continuously updates the flood frequency analysis at all catchments in the world. The model was functioning at the operational level to produce the flood map.

d. *NWM coupled with HAND*

As a part of the National Flood Interoperability Experiment (Maidment 2017), the NOAA National Water Center has been exploring to couple the NWM and HAND to provide the flood map and prediction. The NWM is a specific configuration of the WRF-Hydro model (Cohen et al. 2018), which was originally developed as a land surface model to couple with the Weather Research and Forecasting (WRF) Model (Gochis and Chen 2003). The NWM is based on the Noah-MP land surface model and Muskingum 1D water routing (McCarthy 1939), which emphasizes the energy flux and evapotranspiration process, and uses Phillip's equation to model the infiltration process through conceptual three-layers soil (Niu et al. 2011; Schaake et al. 1996). The simulated 1D flowrate is then fed into HAND for inundation simulation. The HAND 2D flood modeling method created a normalized HAND DEM from the original DEM, which indicates the height of each grid above its nearest flow channel. Then the NWM streamflow data at each drainage reach is converted to the water stage long the channel grids by reversing the flow-stage rating curve, and then any HAND DEM grid values that is small than its nearest water channel stage is considered "wet" and the inundation depth is equal to the difference between the stage and the HAND DEM cell value. The sciences of the NWM+HAND coupled scheme suggest that the method is designed to simulate the fluvial flood only. This simple and conceptual approach was executed at one-third arc second spatial resolution for every day during and after Hurricane Harvey (28 August–3 September 2017). A maximum extent flood simulation was generated based on the daily inundation data and was downloaded from HydroShare platform (Arctur et al. 2018). NWM v1.1 was deployed for operational uses to NCEP from late 2016 until October 2017, when the v1.2 was delivered. These data are based on the NWM v1.1, which includes over 49 000 catchments, and the Harris County, Texas, area had high positive bias but high correlation coefficient when compared with USGS during an official assessment during the NWM training seminar in 2017 (Gochis et al. 2017).

e. *Reference flood data*

Following Hurricane Harvey, the USGS field team visited multiple impact areas and collected over 2000 HWMs with the official guidelines (Feaster and Koenig 2017; Koenig et al. 2016). The HWM ground survey was conducted by measuring the GPS elevation of the mud, debris, and water stain lines on the side of buildings, trees, fences, poles, and other structures. (Watson et al. 2018) utilized over 2000 HWMs and 47 peak stage heights and interpolated them into a flooded water plain at 19 locations, aided by a LiDAR-derived DEM with 1.4–3.0-m resolution. This interpolation result was believed to be the best reconstruction of the flood extent and has been used as a benchmark in another study (Wing et al. 2019). However, this dataset is not error free, and (Watson et al. 2018) indicated the uncertainty ranged from 0.01 to 0.55 m at specific points. These data were obtained from the USGS data release (https://doi.org/10.5066/F7VH5N3N).

Remote sensing technology provide another potential reference for flood extent because there are clear synthetic aperture radar (SAR) images on 29 and 30 August 2017 that capture the Hurricane Harvey and its flooding impact on Harris County (Shen et al. 2019a). Because satellite data can

TABLE 1. List of statistical metrics used in this study. Variables F and f represent the model simulation results of binary classification and values, respectively; R and r represent the reference data of binary classification and values, respectively; 1 and 0 mean positive (wet) and negative (dry) classifications; and n and N represent sample index and a total number of samples.

Name	Equation[a]	Value range	Perfect value
Probability of detection	$\mathrm{POD} = \dfrac{F_1 \wedge R_1}{F_1 \wedge R_1 + F_0 \wedge R_1}$	0, 1	1
False alarm rate	$\mathrm{FAR} = \dfrac{F_1 \wedge R_0}{F_1 \wedge R_0 + F_0 \wedge R_0}$	0, 1	0
Critical success index	$\mathrm{CSI} = \dfrac{F_1 \wedge R_1}{F_1 \wedge R_1 + F_0 \wedge R_1 + F_1 \wedge R_0}$	0, 1	1
Correlation coefficient	$\mathrm{CC} = \dfrac{\sum_{n=1}^{N}(f_n - \bar{f})(r_n - \bar{r})}{\sqrt{\sum_{n=1}^{N}(f_n - \bar{f})^2}\sqrt{\sum_{n=1}^{N}(r_n - \bar{r})^2}}$	−1, 1	1
Root-mean-square error	$\mathrm{RMSE} = \sqrt{\dfrac{1}{N}\sum_{n=1}^{N}(f_n - r_n)^2}$	0, +∞	0

objectively illuminate Earth's surface, they theoretically should be the unbiased ground truth for the flood extent, but only if the information can be extracted accurately. The flood map produced from the Radar-Produced Inundation Diary (RAPID) system in this study was retrieved from Sentinel-1 SAR data captured on 29 August 2017, and then went through the binary classification, morphological processing, compensation, and machine learning correction. The automated algorithms to detect water surface through vegetations and urban structure are not available when RAPID was put online, so RAPID is not capable to extract flood maps in dense metropolitan and heavily vegetated area. The RAPID system was calibrated using a 2016 flooding event in China before processing the data for Hurricane Harvey. The data were obtained from the University of Connecticut Hydrometeorology and Hydrologic Remote Sensing Group RAPID flood map archive (https://rapid-nrt-flood-maps.s3.amazonaws.com/index.html#RAPID_Archive_Flood_Maps/20170829/flooding_S1A_IW_GRDH_1SDV_20170829T002645_20170829T002710_018131_01E74D_3220/). RAPID is an operational system designed to quickly extract flood maps from SAR images during or after the event; therefore, many newer water identification technologies are not incorporated in the system. The RAPID flood map was interpolated using the Floodwater Depth Estimation Tool, version 2 (FwDET v2; Cohen et al. 2019), to generate the flood depth by subtracting the elevation surface created by the edge of the flooded polygon by the 10-m-resolution DEM.

f. Statistical metrics

Two levels of statistical tests were used in the evaluation. First, the reference data from section 2e were used to test the extent to which the models capture the spatial patterns of flooding. In this case, we used standard binary pattern measures listed in Table 1.

The probability of detection (POD) measures the model's ability to capture the referencing flood extent or the proportion of the reference flood extent that was replicated by the model. The false alarm rate (FAR) reflects the model's tendency to overestimate the reference flood extent or the proportion of the modeled flood area that was classified as positive while the reference data were classified as negative. The critical success index (CSI) measures performance of the model estimates relative to the reference flood extent, which accounts for both overprediction and underprediction by the model.

Second, the 50 USGS HWMs in the study area were used as the reference to calculate the difference produced by the model simulations. Two metrics were used (Table 1), where the correlation coefficient measures the relationships between model-simulated inundation depth and HWMs and root-mean-square error (RMSE) measures the average magnitude of the errors from the model simulations. These traditional statistics test if the models capture the pattern and accurate water inundation depth.

3. Results and discussion

a. Flood extent evaluation

A display of flood maps from the USGS mapping, SAR data interpolation, NWM+HAND, Fathom (LISFLOOD-FP), and CREST-iMAP are listed in Fig. 3. To visually compare all datasets, all data were cropped within the USGS HWMs' interpolation boundaries, and the maximum values of each pixel in the modeled time series were taken from the model outputs. For ease of observing, only inundation-depth pixel values that are larger than 1 in. (0.0254 m) was displayed in Fig. 3.

The satellite-based flood mapping was not able to capture most of the flood inundation as compared with other methods. Therefore, the satellite-based flood mapping failed in this study area and will not be included for further analysis. However, the SAR data captures a small area of flood at the southwestern corner of the boundary (green line), which indicates that the SAR and RAPID system performs slightly better at the ranch area instead of mountainous or urban area. The NWM+HAND method has a very limited flood extent but better than the satellite-based flood mapping. Especially, the NWM+HAND method could not capture the large flooded area at the upper stream of the Cypress Creek (lower-left corner of the study

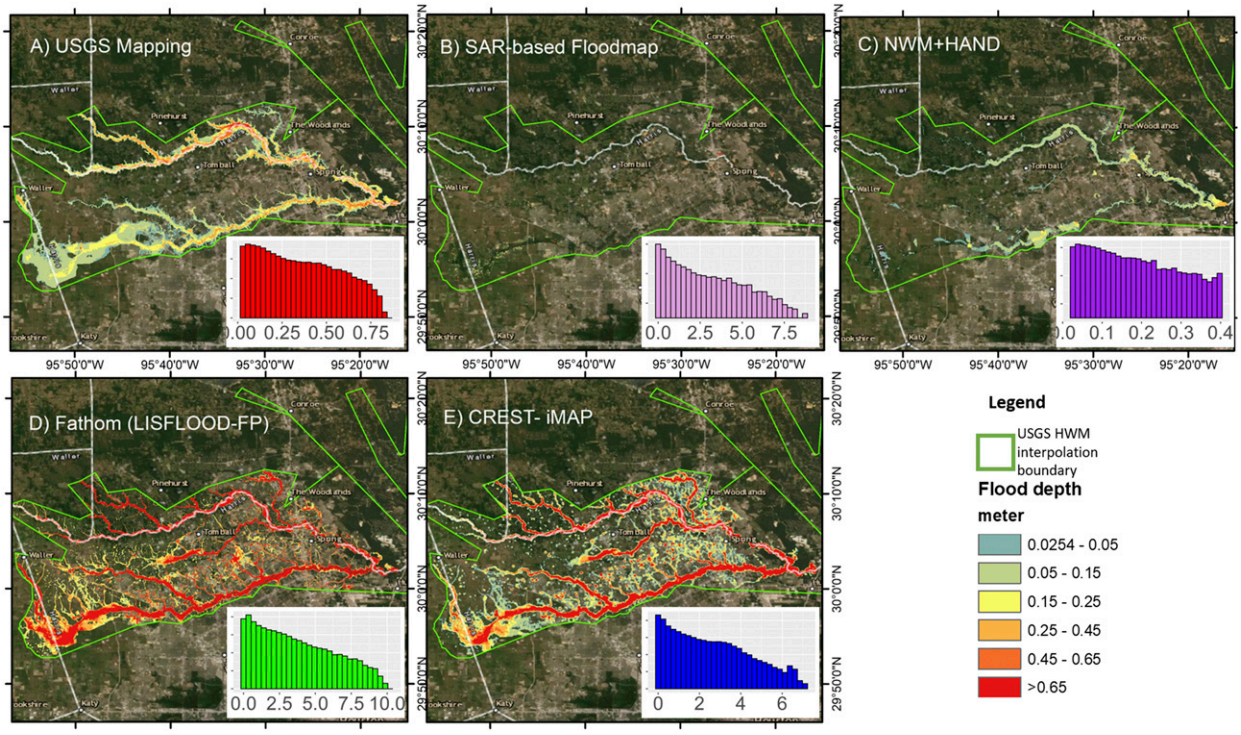

FIG. 3. The flood extent and depth of (a) USGS inundation mapping, (b) SAR-image flood mapping, (c) NWM+HAND, (d) the Fathom model, and (e) the CREST-iMAP model, and their flood-depth distributions.

boundary), where USGS mapping, Fathom and CREST-iMAP all found inundation in the area. The USGS mapping only captures the fluvial flooding along the three main streams (Spring Creek, Cypress Creek, Little Cypress Creek). In contrast, the two modeling methods can capture more inundation along smaller channels. The major flooding occurred at the southwestern side of the basin, which was captured by the two simulations and the USGS interpolation. However, by looking at the flood-depth distribution at subplots and the color scales of each map, the simulated inundation depths are very different as the Fathom simulation output appears to have more ''red'' pixels than the other methods and its maximum inundation depth reaches over 10 m. Note that the NWM+HAND method produced eight ''noise'' pixels that have values around 11 m while the majority of the pixel values are less than 0.4 m, which can be caused by the DEM error or during the data processing. One observation of the different flood maps is that the maximum flood depth ranges from 0.4 to >10 m, where the USGS mapping, Fathom, and CREST-iMAP all include the channel water depth while SAR and NWM+HAND do not. The variation of flood depth can be caused by the different DEM treatments by each automated operating system, even though all automated methods use the DEM from the USGS National Elevation Dataset. Fathom has river channels ''burned'' into the DEM, whereas CREST-iMAP uses the native DEM and SAR flood map interpolation and NWM+HAND uses ditch-filled DEM. The benchmark USGS flood map uses its own lidar-detected data as DEM, which is unique and different from all other methods. A more detailed flood-depth analysis will be done in section 3b.

Assuming the USGS flood mapping is the ground truth and is set as the benchmark of the study and that only over 1 in. (2.54 cm) of water depth is considered as an inundated pixel, the comparison results are listed in Table 2. The previous study indicated that Spring Creek and the San Jacinto River area were one of the poor-performance basins (Wing et al. 2019). This study confirmed the performance where the POD indicates 72% of the area matched the benchmark, and the CSI was only 0.49. The CREST-iMAP has a comparable performance, where the POD was 72%, and CSI was 0.45. Both models produced false alarms, and their FARs were over 40%, which was caused by the large underrepresentation of pluvial flooding between the two main streams according to the benchmark USGS flood map (Fig. 4. Blue area). Relative to the other two models, the NWM+HAND approach dramatically underperformed, giving only 22% detection, and the CSI is only 0.21.

TABLE 2. The comparison results of NWM+HAND, Fathom (LISFLOOD-FP), and CREST-iMAP with the benchmark USGS flood mapping. The POD, FAR, and CSI were described in section 2 and Table 1, with the threshold of 1 in. (2.54 cm).

Name	NWM+HAND	Fathom	CREST-iMAP
POD	0.22	0.72	0.72
FAR	0.13	0.40	0.45
CSI	0.21	0.49	0.45

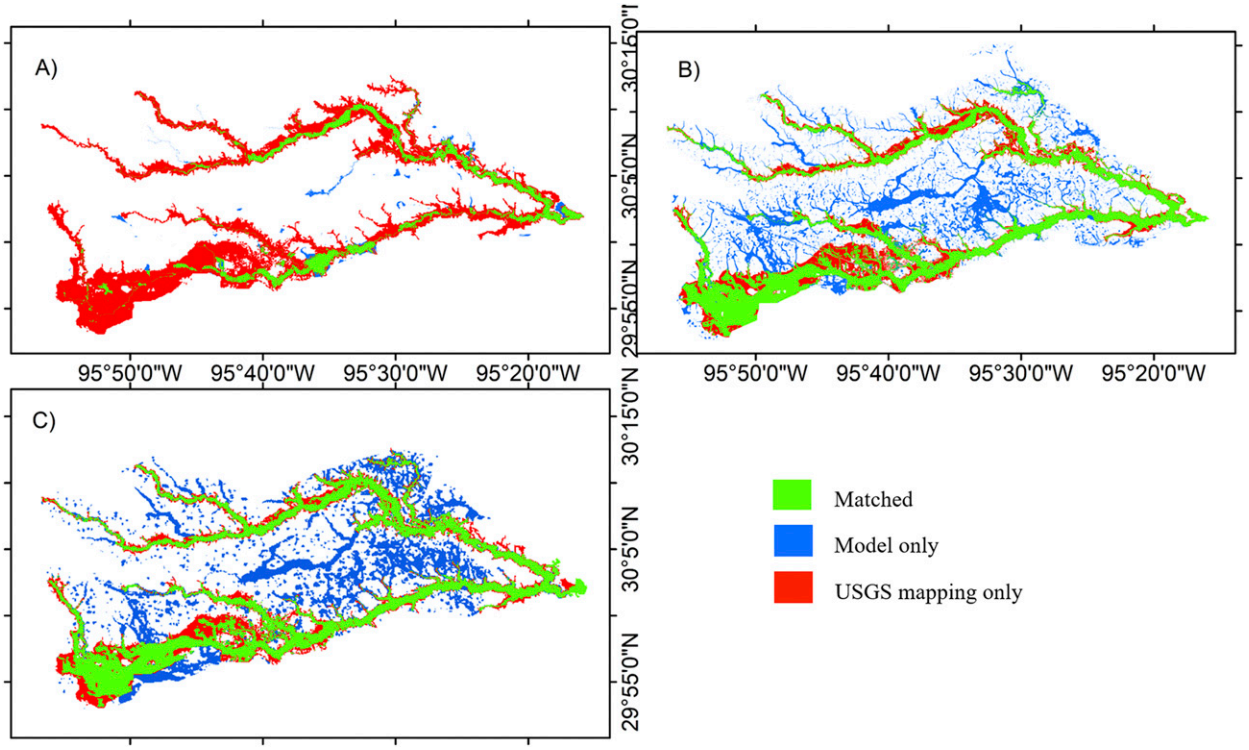

FIG. 4. Maps displaying the intersection of the (a) NWM+HAND, (b) Fathom, and (c) CREST-iMAP flood extents with those from the USGS flood mapping.

Because the NWM+HAND simulated flooded area is very small, the FAR is as low as 13%.

Figure 4 demonstrates the spatial distribution of the match between the model simulations and the USGS flood map. The NWM+HAND shows clear underestimation where only the center lines of the two main downstreams appear to have inundations, and all the upper streams flooding are not captured. Since NWM-HAND only considers the overbank flow, there is no pluvial flood showing between two main streams, which leads to the low FAR value. Besides the large false alarms from Fathom and CREST-iMAP models, the general performance over two major streams appears to be good. CREST-iMAP performed better than Fathom on Spring Creek (northern stream), and Fathom performed better at the upper part of Cypress Creek (southern stream) than CREST-iMAP. Both model simulations did not fully capture the east end of the upper Cypress Creek flood, where Cypress City is located (29.98°N, 95.74°W). The CREST-iMAP simulation showed a more inundated area in the eastern portion of the study area, which is more developed and lower in elevation. Fathom simulation showed more flooding at the middle and upper streams of the study area, especially along the flowlines and small water channels.

It is reasonable to raise speculations about how underrepresentative the USGS flood mapping was for Hurricane Harvey. First, the method of the USGS flood mapping does not consider any physical water movement nor hydrological cycling dynamics. Second, both models showed a significant amount of false alarms in the area between two major rivers, which indicates the benchmark data might be underrepresenting. To investigate further, we counted the number of FEMA flood/water damage insurance claims that landed on the ''wet'' pixels of different flood maps. The results are illustrated in Fig. 5.

The flood/water damage insurance claims included water damages, flood, water-related electrical damages, and property rupture or cracks, with a total of 10,459 cases within the study area. Since it is difficult to determine how much water could cause water damage, any pixel has value more than 0 m was considered as a wet area for all datasets. The satellite-based flood map is very sparse, so there were only 107 (1.0%) claims collocated with the flood extent. The NWM+HAND is proven to underestimate the flooding by Hurricane Harvey, and there were only 1692 (16.2%) claims inside the simulated flood extent. For the USGS flood map, there were 4610 (44.1%) claims inside its flood extent approximation, which is mainly aligning along the two main river channels, as the USGS interpolation heavily focused on the fluvial flooding. The Fathom simulated flood extent has number of claims that is comparable to USGS mapping of 4284 (41.0%). However, the claims associated with flooded pixels in the Fathom simulation are visually more widespread when compared with the USGS map, where it shows many more claims between the two main rivers (Fig. 5c). We speculate that since no model simulation showed as much flood inundation area at the City of Cypress as the USGS mapping, concentrated flood/water damage claims (1896 out of

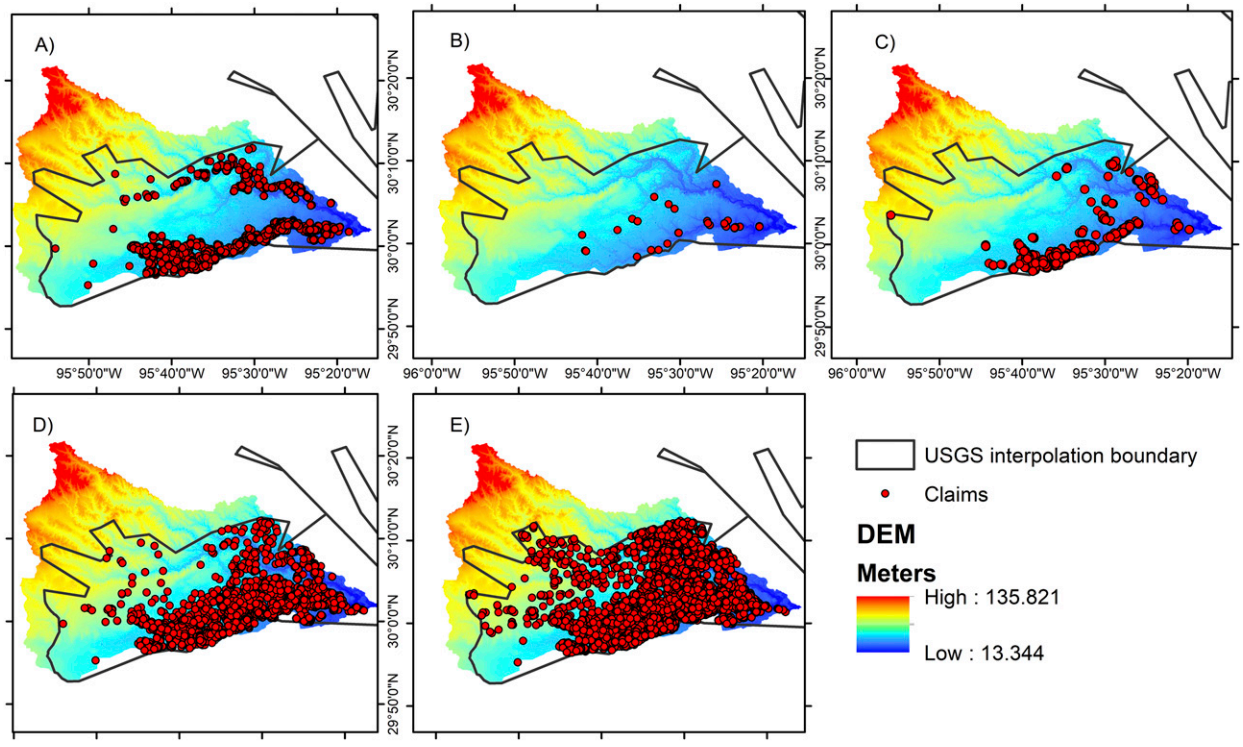

FIG. 5. The filed FEMA flood/water damage insurance claims that land within the "wet" area from each flood-mapping source: (a) USGS flood mapping, (b) satellite-based flood extent, (c) NWM+HAND, (d) Fathom model simulation, and (e) CREST-iMAP model simulation.

10 459 claims) were partially counted in the Fathom simulation. Therefore, even though Fig. 5c visually shows more widespread claims, the USGS flood map has a higher count of claims associated to inundated pixels. The CREST-iMAP simulated flood extent contains the most claims of 9085 (86.9%), which indicates the benefit of the full pluvial flood simulation scheme can better capture the extreme precipitation triggered flood inundation. From Fig. 5e, the claim points are well spread across the study area, and especially in the northern river, Spring Creek, the model simulation captured more flood/water damage insurance claims than all other methods.

Overall, it is difficult to conclude which flood prediction method is better than others or which methods can better be used as the benchmark data that represent the ground truth during the event. In theory, the satellite-based (SAR) flood map should have provided the "ground truth" because the data were derived from the snapshot when Sentinel-1 passed over the area on 29 August 2017 (Shen et al. 2019a). According to the CREST-iMAP simulated results, the study area had the most wet pixels at 1145 UTC 29 August 2017 during Hurricane Harvey, which is consistent with the date of the peak USGS gauged and EF5 simulated streamflow in a previous study (Chen et al. 2020). However, the SAR flood map shows the SAR and RAPID method only captures very small flood inundation at the southwestern ranches of the study area. As the water detection through vegetation and urban buildings from SAR data is not available for an automated system like RAPID, the lack of flood extent detection exposes the limitation of the satellite-based automated flood-mapping system when detecting through large objects is not available. The USGS flood map has been used as the benchmark in other studies, but it is unrealistic to have no inundation away from the river channels, and only less than half (44.1%) of the flood insurance claims landed within its flood extent.

The NWM+HAND method underperforms, but the data were generated by NWM v1.1, and, as of today, the model has developed to v2.0 and v2.1, which we believe should have better performance now. However, this NWM+HAND is still limited to the stage-flow conversion, DEM manipulation, and other systematic errors (Johnson et al. 2019). The Fathom- and CREST-iMAP-simulated flood extents showed promising results that can capture the pluvial flood. However, Fathom's simulation of flood extent captures less inundation at the downstream of the basin and around Spring Creek, which leads to fewer insurance cases within its flood extent (41%) relative to USGS mapping and CREST-iMAP simulation. The Fathom system uses the return period of the streams as the main forcing to the model, and the infiltration capacity method might undermine the effects of the overland flow and subsurface flow. Meanwhile, LISFLOOD-FP uses local inertial method to simplify the St. Venant shallow-water equation, which requires individual flood surveyed flood extent for each catchment for calibration to reach optimal result, but it is hard to achieve for a

continental scale, automated operational flood model (Horritt and Bates 2002).

The CREST-iMAP shows the broadest coverage over insurance claims in the basin (80+ %). At the same time, the FAR (45%) is similar to the Fathom simulation (FAR = 40%) when compared with the USGS flood map, which means that the CREST-iMAP simulation has an amount of overestimation that is comparable to the other modeling approach in this study. Therefore, it is reasonable speculation that the CREST-iMAP simulation can cover the majority of the flood insurance claim is due to the better description of the water movements during Hurricane Harvey, by using the fully solved shallow-water equation instead of the simplified local inertial form in Fathom or a conceptual interpolation used in HAND. The CREST-iMAP uses the 2-min MRMS QPE as the model forcing data, which contains errors that can propagate through the flood simulations and it is not treated in this study as a hypothetical automated operating test. Both Fathom and CREST-iMAP do not represent the mid- and upper Cypress Creek flood very well, relative to the USGS flood map, which is where the city of Cypress is located. This shows a certain degree of inability of simulating urban flooding by automated flood modeling, since Cypress was heavily flooded during Hurricane Harvey according to news reporting and social media posts.

The flood extent analysis shows that the CREST-iMAP model at its current setting has a result that is comparable to the operational Fathom system, in comparison with the benchmark USGS flood map, which also matches well with FEMA flood insurance claims. The flood extent from SAR and NWM+HAND are shown to be underrepresentative.

b. *Flood inundation-depth analysis*

The model simulated inundation-depth values were extracted from the same locations as the 50 HWM sites in the study area. Figure 6 shows the water depths at each location from different data sources.

The first observation from the result is that the Fathom-simulated flood depth has much higher extreme values relative to other sources, which is consistent with the results in Fig. 3 where Fathom has more red area and its inundation value has the largest range among all flood approximations. The error distribution of Fathom simulation also indicates that there are multiple pixels overestimate the flood depth by 2–4 m. Second, considering NWM+HAND does not have pixel values at 31 locations, the rest of the locations appears to slightly overestimate the flood depth, with two extreme values (error > 7 m) that are beyond the range of the figure. Third, no flood inundation data source aligns perfectly with the USGS HWM measurement, and CREST-iMAP is the only model that limits the majority of the error within ± 2 m. Therefore, no modeling method can approximate the actual ground survey in this study, which leaves room for much improvement in the field. The statistical analysis was done to analyze and compare the simulated data with the USGS HWM as the reference (Table 3).

The results indicate that all flood inundation-depth approximations have poor correlation with the USGS HWM records (<0.51) and about 1 m of error. Despite the fact that there are 31 no-value pixels extracted at HWM locations from the NWM+HAND simulation result, its depth is the most correlated with the ground survey with CC of 0.51 but is the least accurate with RMSE of 1.81 m. The CREST-iMAP model simulation has a less-poor performance, with CC of 0.36 and RMSE of 0.91 m. The Fathom simulation yields an RMSE of 1.26 and CC of 0.12, which indicates that the water-depth simulation is not valid. The scatterplot (Fig. 7) shows the concentration of Fathom simulation results close to the upper-left corner, which indicates that the majority of overestimation occurs when the inundation water depth is less than 1 m. All flood simulation methods yield overestimation when the HWM value is 0 (a very small flood inundation), and Fathom tends to have greater flood-depth values than CREST-iMAP and NWM+HAND. Majority of the overestimation of CREST-iMAP occur at the locations with 0 value HWMs and many underestimations occur at the locations when HWMs are between 0.5 and 1.5 m.

Overall, the correlations between the USGS HWM and different flood-mapping approximations were low, where there is no clear pattern along the isoline in this scatterplot. It is partially due to the inaccuracy of the flood inundation simulations, as well as the USGS HWM measurements, which is based on human observation and claims the uncertainty is between ± 0.015 m (0.05 ft) and ± 0.12 m (0.4 ft) (Feaster and Koenig 2017). Another reason could be the location information of the HWM sites is not accurate enough, which the USGS HWM dataset provide the longitude and latitude coordinates at accuracy of five digits after the decimal point. However, all flood simulation models were operated under hyper-resolution (3–10 m). Therefore, only 10^{-5} arc-degree accuracy is not enough to precisely extract the right pixel from the modeled flood inundation result, which could cause the inconsistency that we found this study. The previous Hurricane Harvey study (Wing et al. 2019) also argued that the Fathom model error relative to HWM was close to 1.19 m and justified that the ~1-m model deviation from the HWM was acceptable and informative to flood prevention and preparations for local first responders. This study provides another flood inundation approximation method that marginally improved the error (RMSE) to ~0.9 m.

4. Conclusions

Validation of a flood map for a single event is challenging because error-free reference data that comprehensively reflect a flood event are not available. This is especially true in this study, and none of the flood maps can be proven to be the unbiased ground truth. This study also provides a model application that couples the hydrological and hydraulic model using excessive rainfall as the media dataset. The results prove that the CREST-iMAP framework can well capture the flood extent and the spatial pattern of the flood extent, which is comparable to current automated operational flood-monitoring systems in the world. However, the error (RMSE) is approximately 0.9 m using the traditional statistical method. This study compares the five different sources of flood inundation approximations for the flood

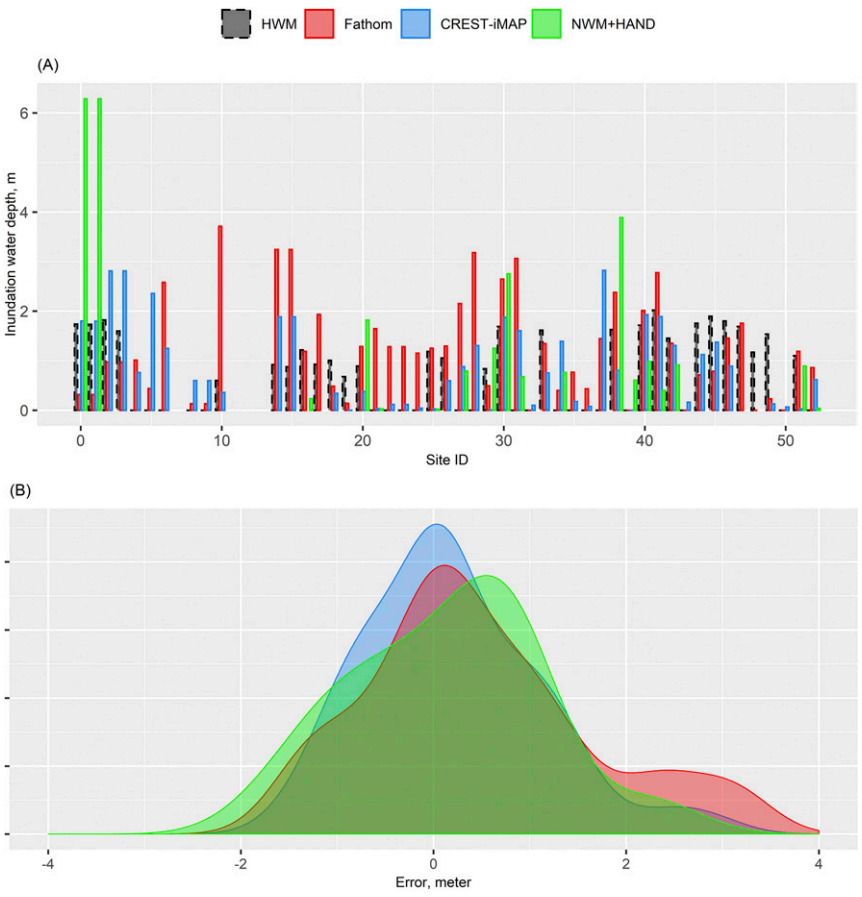

FIG. 6. The (a) flood inundation depth at 50 USGS HWM locations, and (b) error distributions of the NWM+HAND simulation, Fathom simulation, and CREST-iMAP simulation.

induced by Hurricane Harvey in Spring Basin located in northern Harris County: RAPID extraction from SAR data, USGS HWM and stream stage interpolation, NWM+HAND model simulation, Fathom (LISFLOOD-FP) model simulation, and CREST-iMAP model simulation. The main conclusions of this study are 1) the CREST-iMAP modeling methods can capture the flood extent under extreme precipitation as well, if not better than, as other sources, 2) satellite-based (SAR) flood observation and NWM+HAND model simulation severely underperformed during Hurricane Harvey and HAND only considers the fluvial flood, and 3) this study cannot conclude which is the most reliable method to capture the flood inundation during the extreme event because no method can completely reproduce the flood extent and the inundation-depth errors are not negligible.

This study provides a hydrological and hydraulic coupled approach to simulate flooding with fewer data requirements in an automated and operational setup using the CREST-iMAP framework, which yields acceptable results during the Hurricane Harvey extreme precipitation-driven flood event. The current case study has 41 million computing pixels and a computational speed of 0.02 s per time step (10 s) using 2 nodes (40 computing cores), but a more systematic computational efficiency study for the CREST-iMAP will be needed in the future. Even though the simulated flood depth is not perfect, there is plenty of decision-supportive information to potentially establish a high-resolution flood prediction system based on the weather radar network for not only southeastern Texas but along all high-precipitation intensity and flood-prone areas across the globe, because the model is physics based, is compatible with global data, and is built with a parameter regionalization module. Furthermore, because the CREST-iMAP framework can comprehensively provide streamflow, flood extent, flood inundation depth, and soil moisture outputs, it can easily connect to other interdisciplinary building blocks

TABLE 3. Traditional statistical analysis of the HWM+HAND simulation, Fathom (LISFLOOD-FP) simulation, and CREST-iMAP simulation. The CC and RMSE were described in section 2 and Table 1. Here, NA indicates no available data.

Name	NWM+HAND	Fathom	CREST-iMAP
CC	0.51	0.12	0.38
RMSE (m)	1.81	1.26	0.91
No. of NAs	31	1	1

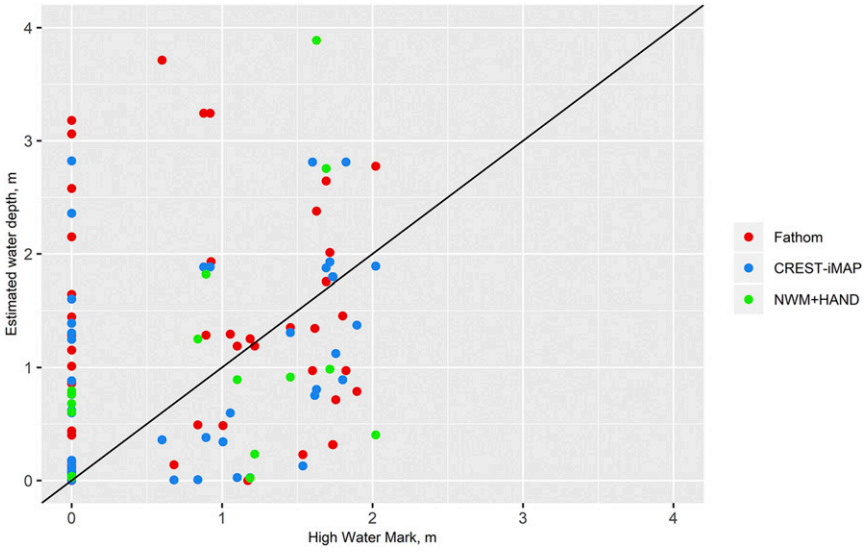

FIG. 7. The scatterplot of NWM+HAND (green), the Fathom (LISFLOOD-FP) simulation (red), and the CREST-iMAP simulation (blue) compared with 50 USGS HWM records as the reference.

(e.g., insurance, supply chain, and utility management) to further quantify the consequential socioeconomic impacts from any flood event. Ultimately, a decision-supporting smart system can be built upon reliable flood predictions to guide public safety decision-making during flood hazards.

Acknowledgments. The authors are thankful for the support from Oklahoma University Hydrology and Water Security program.

Data availability statement. The authors were unable to find a valid data repository for the data used in this study. These data are available by contacting the first author Mengye Chen: mchen15@ou.edu.

REFERENCES

Adhikari, P., Y. Hong, K. R. Douglas, D. B. Kirschbaum, J. J. Gourley, R. Adler, and G. R. Brakenridge, 2010: A digitized global flood inventory (1998-2008): Compilation and preliminary results. *Nat. Hazards*, **55**, 405–422, https://doi.org/10.1007/s11069-010-9537-2.

Alcrudo, F., 2004: A state of the art review on mathematical modelling of flood propagation. EVG1-CT-2001-00037, 22 pp., https://cupdf.com/document/a-state-of-the-art-review-on-mathematical-modelling-of-flood-propagation-first.html.

Anselmo, V., G. Galeati, S. Palmieri, U. Rossi, and E. Todini, 1996: Flood risk assessment using an integrated hydrological and hydraulic modelling approach: A case study. *J. Hydrol.*, **175**, 533–554, https://doi.org/10.1016/S0022-1694(96)80023-0.

Arctur, D., E. Boghichi, D. Tarboton, D. Maidment, J. Bales, R. Idaszak, M. Seul, and A. M. Castronova, 2018: Hurricane Harvey 2017 Collection. Hydroshare, accessed 18 January 2018, https://doi.org/10.4211/hs.2836494ee75e43a9bfb647b37260e461.

Ashley, S. T., and W. S. Ashley, 2008: Flood fatalities in the United States. *J. Appl. Meteor. Climatol.*, **47**, 805–818, https://doi.org/10.1175/2007JAMC1611.1.

Barredo, J. I., 2007: Major flood disasters in Europe: 1950-2005. *Nat. Hazards*, **42**, 125–148, https://doi.org/10.1007/s11069-006-9065-2.

Bates, P. D., and A. P. J. De Roo, 2000: A simple raster-based model for flood inundation simulation. *J. Hydrol.*, **236**, 54–77, https://doi.org/10.1016/S0022-1694(00)00278-X.

——, M. S. Horritt, and T. J. Fewtrell, 2010: A simple inertial formulation of the shallow water equations for efficient two-dimensional flood inundation modelling. *J. Hydrol.*, **387**, 33–45, https://doi.org/10.1016/j.jhydrol.2010.03.027.

Benito, G., and Coauthors, 2004: Use of systematic, palaeoflood and historical data for the improvement of flood risk estimation. Review of scientific methods. *Nat. Hazards*, **31**, 623–643, https://doi.org/10.1023/B:NHAZ.0000024895.48463.eb.

Blake, E. S., and D. A. Zelinsky, 2018: National Hurricane Center tropical cyclone report Hurricane Harvey (AL092017). National Hurricane Center Rep., 77 pp., https://www.nhc.noaa.gov/data/tcr/AL092017_Harvey.pdf.

Brauer, N. S., J. B. Basara, C. R. Homeyer, G. M. McFarquhar, and P. E. Kirstetter, 2020: Quantifying precipitation efficiency and drivers of excessive precipitation in post-landfall Hurricane Harvey. *J. Hydrometeor.*, **21**, 433–452, https://doi.org/10.1175/JHM-D-19-0192.1.

Brunner, G. W., 2016: HEC-RAS River Analysis System hydraulic reference manual version 5.0. U.S. Army Corps of Engineers Hydrologic Engineering Center Doc. CPD-69, 538 pp., https://www.hec.usace.army.mil/software/hec-ras/documentation/HEC-RAS%205.0%20Reference%20Manual.pdf.

Chen, M., S. Nabih, N. S. Brauer, S. Gao, J. J. Gourley, Z. Hong, R. L. Kolar, and Y. Hong, 2020: Can remote sensing technologies capture the extreme precipitation event and its cascading hydrological response? A case study of hurricane Harvey using EF5 modeling framework. *Remote Sens.*, **12**, 445, https://doi.org/10.3390/rs12030445.

Clark, R. A., and Coauthors, 2017: Hydrological modeling and capacity building in the Republic of Namibia. *Bull. Amer. Meteor. Soc.*, **98**, 1697–1715, https://doi.org/10.1175/BAMS-D-15-00130.1.

Cohen, S., S. Praskievicz, and D. R. Maidment, 2018: Featured collection introduction: National water model. *J. Amer. Water Resour. Assoc.*, **54**, 767–769, https://doi.org/10.1111/1752-1688.12664.

——, and Coauthors, 2019: The Floodwater Depth Estimation Tool (FwDET v2.0) for improved remote sensing analysis of coastal flooding. *Nat. Hazards Earth Syst. Sci.*, **19**, 2053–2065, https://doi.org/10.5194/nhess-19-2053-2019.

de Almeida, G. A. M., and P. Bates, 2013: Applicability of the local inertial approximation of the shallow water equations to flood modeling. *Water Resour. Res.*, **49**, 4833–4844, https://doi.org/10.1002/wrcr.20366.

Dickinson, R. E., R. M. Errico, F. Giorgi, and G. T. Bates, 1989: A regional climate model for the western United States. *Climatic Change*, **15**, 383–422, https://doi.org/10.1007/BF00240465.

Feaster, T. D., and T. A. Koenig, 2017: Field manual for identifying and preserving high-water mark data. U.S. Geological Survey, 80 pp., https://pubs.usgs.gov/of/2017/1105/ofr20171105.pdf.

Flamig, Z. L., H. Vergara, and J. J. Gourley, 2020: The Ensemble Framework For Flash Flood Forecasting (EF5) v1.2: Description and case study. *Geosci. Model Dev.*, **13**, 4943–4958, https://doi.org/10.5194/gmd-13-4943-2020.

Ghimire, B., A. S. Chen, M. Guidolin, E. C. Keedwell, S. Djordjević, and D. A. Savić, 2013: Formulation of a fast 2D urban pluvial flood model using a cellular automata approach. *J. Hydroinfo.*, **15**, 676–686, https://doi.org/10.2166/hydro.2012.245.

Gochis, D. J., and F. Chen, 2003: Hydrological enhancements to the Community Noah Land Surface Model. NCAR/TN-454+STR, UCAR/NCAR, 77 pp., https://opensky.ucar.edu/islandora/object/technotes%3A373/datastream/PDF/view.

——, and Coauthors, 2017: The NOAA National Water Model: Research to operations to research. CUAHSI Presentation, 62 pp., https://www.cuahsi.org/uploads/cyberseminars/David_Gochis_Presentation.pdf.

Gourley, J. J., and Coauthors, 2017: The Flash Project: Improving the tools for flash flood monitoring and prediction across the United States. *Bull. Amer. Meteor. Soc.*, **98**, 361–372, https://doi.org/10.1175/BAMS-D-15-00247.1.

Hong, Y., K.-L. Hsu, H. Moradkhani, and S. Sorooshian, 2006: Uncertainty quantification of satellite precipitation estimation and Monte Carlo assessment of the error propagation into hydrologic response. *Water Resour. Res.*, **42**, W08421, https://doi.org/10.1029/2005WR004398.

Horritt, M. S., and P. D. Bates, 2002: Evaluation of 1D and 2D numerical models for predicting river flood inundation. *J. Hydrol.*, **268**, 87–99, https://doi.org/10.1016/S0022-1694(02)00121-X.

Johnson, J. M., D. Munasinghe, D. Eyelade, and S. Cohen, 2019: An integrated evaluation of the National Water Model (NWM)–Height Above Nearest Drainage (HAND) flood mapping methodology. *Nat. Hazards Earth Syst. Sci.*, **19**, 2405–2420, https://doi.org/10.5194/nhess-19-2405-2019.

Koenig, T. A., and Coauthors, 2016: Identifying and preserving high-water mark data. U.S. Geological Survey Techniques and Methods Rep. 3-A24 (chap. 24 of section A, Surface water techniques, of book 3, Applications of Hydraulics), 47 pp., https://pubs.usgs.gov/tm/03/a24/tm3a24.pdf.

Kossin, J. P., 2018: A global slowdown of tropical-cyclone translation speed. *Nature*, **558**, 104–107, https://doi.org/10.1038/s41586-018-0158-3.

Lehner, B., K. Verdin, and A. Jarvis, 2008: New global hydrography derived from spaceborne elevation data. *Eos, Trans. Amer. Geophys. Union*, **89**, 93, https://doi.org/10.1029/2008EO100001.

Lejot, J., C. Delacourt, H. Piégay, T. Fournier, M.-L. Trémélo, and P. Allemand, 2007: Very high spatial resolution imagery for channel bathymetry and topography from an unmanned mapping controlled platform. *Earth Surf. Processes Landforms*, **32**, 1705–1725, https://doi.org/10.1002/esp.1595.

Li, Z., M. Chen, S. Gao, Z. Hong, G. Tang, Y. Wen, J. J. Gourley, and Y. Hong, 2020: Cross-examination of similarity, difference and deficiency of gauge, radar and satellite precipitation measuring uncertainties for extreme events using conventional metrics and multiplicative triple collocation. *Remote Sens.*, **12**, 1258, https://doi.org/10.3390/rs12081258.

Liang, X., D. P. Lettenmaier, and E. F. Wood, 1996a: One-dimensional statistical dynamic representation of subgrid spatial variability of precipitation in the two-layer variable infiltration capacity model. *J. Geophys. Res.*, **101**, 21 403–21 422, https://doi.org/10.1029/96JD01448.

——, E. F. Wood, and D. P. Lettenmaier, 1996b: Surface soil moisture parameterization of the VIC-2L model: Evaluation and modification. *Global Planet. Change*, **13**, 195–206, https://doi.org/10.1016/0921-8181(95)00046-1.

Lighthill, M. J., and G. B. Whitham, 1955: On kinematic waves I. Flood movement in long rivers. *Proc. Roy. Soc. London: Math. Phys. Sci.*, **229A**, 281–316, https://doi.org/10.1098/rspa.1955.0088.

Liu, Z., V. Merwade, and K. Jafarzadegan, 2019: Investigating the role of model structure and surface roughness in generating flood inundation extents using one- and two-dimensional hydraulic models. *J. Flood Risk Manage.*, **12**, e12347, https://doi.org/10.1111/jfr3.12347.

Maidment, D. R., 2017: Conceptual framework for the national flood interoperability experiment. *J. Amer. Water Resour. Assoc.*, **53**, 245–257, https://doi.org/10.1111/1752-1688.12474.

McCarthy, G. T., 1939: *The Unit Hydrograph and Flood Routing*. Army Engineer District, 815 pp.

McDonald, W. M., and J. B. Naughton, 2019: Impact of Hurricane Harvey on the results of regional flood frequency analysis. *J. Flood Risk Manage.*, **12**, e12500, https://doi.org/10.1111/jfr3.12500.

Merwade, V. M., D. R. Maidment, and J. A. Goff, 2006: Anisotropic considerations while interpolating river channel bathymetry. *J. Hydrol.*, **331**, 731–741, https://doi.org/10.1016/j.jhydrol.2006.06.018.

Morin, J., and Y. Benyamini, 1977: Rainfall infiltration into bare soils. *Water Resour. Res.*, **13**, 813–817, https://doi.org/10.1029/WR013i005p00813.

National Weather Service, 2018: Service assessment August/September 2017 Hurricane Harvey. NOAA Rep., 78 pp., https://www.weather.gov/media/publications/assessments/harvey6-18.pdf.

Nielson, O. M., D. Roberts, A. McPherson, and A. Hitchman, 2005: Hydrodynamic modelling of coastal inundation. *MODSIM 2005 Int. Congress on Modelling and Simulation*, A. Zerger and R. M. Argent, Eds., Modelling and Simulation Society of Australia & New Zealand, 518–523.

Niu, G.-Y., and Coauthors, 2011: The community Noah land surface model with multiparameterization options (Noah-MP): 1. Model description and evaluation with local-scale measurements. *J. Geophys. Res.*, **116**, D12109, https://doi.org/10.1029/2010JD015139.

Orzech, M. D., A. J. H. M. Reniers, E. B. Thornton, and J. H. MacMahan, 2011: Megacusps on rip channel bathymetry: Observations and modeling. *Coast. Eng.*, **58**, 890–907, https://doi.org/10.1016/j.coastaleng.2011.05.001.

Rappaport, E. N., 2000: Loss of life in the United States associated with recent Atlantic tropical cyclones. *Bull. Amer. Meteor.*

Soc., **81**, 2065–2073, https://doi.org/10.1175/1520-0477(2000)081<2065:LOLITU>2.3.CO;2.

——, 2014: Fatalities in the United States from Atlantic tropical cyclones: New data and interpretation. *Bull. Amer. Meteor. Soc.*, **95**, 341–346, https://doi.org/10.1175/BAMS-D-12-00074.1.

Roberts, S., O. Nielson, D. Gray, J. Sexton, and G. Davies, 2019: ANUGA user manual release 2.0.3. Commonwealth of Australia (Geoscience Australia) and the Australian National University Rep., 101 pp., https://github.com/GeoscienceAustralia/anuga_core/blob/master/doc/anuga_user_manual.pdf.

Sampson, C. C., A. M. Smith, P. D. Bates, J. C. Neal, L. Alfieri, and J. E. Freer, 2015: A high-resolution global flood hazard model. *Water Resour. Res.*, **51**, 7358–7381, https://doi.org/10.1002/2015WR016954.

Schaake, J. C., V. I. Koren, Q.-Y. Duan, K. Mitchell, and F. Chen, 1996: Simple water balance model for estimating runoff at different spatial and temporal scales. *J. Geophys. Res.*, **101**, 7461–7475, https://doi.org/10.1029/95JD02892.

Shen, X., Y. Hong, K. Zhang, and Z. Hao, 2017: Refining a distributed linear reservoir routing method to improve performance of the CREST model. *J. Hydrol. Eng.*, **22**, 04016061, https://doi.org/10.1061/(ASCE)HE.1943-5584.0001442.

——, E. N. Anagnostou, G. H. Allen, G. Robert Brakenridge, and A. J. Kettner, 2019a: Near-real-time non-obstructed flood inundation mapping using synthetic aperture radar. *Remote Sens. Environ.*, **221**, 302–315, https://doi.org/10.1016/j.rse.2018.11.008.

——, D. Wang, K. Mao, E. Anagnostou, and Y. Hong, 2019b: Inundation extent mapping by synthetic aperture radar: A review. *Remote Sens.*, **11**, 879, https://doi.org/10.3390/rs11070879.

Smith, K., and R. Ward, 1998: *Floods: Physical Processes and Human Impact*. John Wiley and Sons, 382 pp.

Syvitski, J. P. M., and G. R. Brakenridge, 2013: Causation and avoidance of catastrophic flooding along the Indus River, Pakistan. *GSA Today*, **23**, 4–10, https://doi.org/10.1130/GSATG165A.1.

Tanaka, T., H. Yoshioka, S. Siev, H. Fujii, Y. Fujihara, K. Hoshikawa, S. Ly, and C. Yoshimura, 2018: An integrated hydrological-hydraulic model for simulating surface water flows of a shallow lake surrounded by large floodplains. *Water*, **10**, 1213, https://doi.org/10.3390/w10091213.

Teng, J., A. J. Jakeman, J. Vaze, B. F. W. Croke, D. Dutta, and S. S. H. Kim, 2017: Flood inundation modeling: A review of methods, recent advances and uncertainty analysis. *Environ. Modell. Software*, **90**, 201–216, https://doi.org/10.1016/j.envsoft.2017.01.006.

van Oldenborgh, G. J., and Coauthors, 2018: Corrigendum: Attribution of extreme rainfall from Hurricane Harvey, August 2017. *Environ. Res. Lett.*, **13**, 019501, https://doi.org/10.1088/1748-9326/aaa343.

Vergara, H., P. E. Kirstetter, J. J. Gourley, Z. L. Flamig, Y. Hong, A. Arthur, and R. L. Kolar, 2016: Estimating a-priori kinematic wave model parameters based on regionalization for flash flood forecasting in the Conterminous United States. *J. Hydrol.*, **541**, 421–433, https://doi.org/10.1016/j.jhydrol.2016.06.011.

Vrugt, J. A., 2016: Markov chain Monte Carlo simulation using the DREAM software package: Theory, concepts, and MATLAB implementation. *Environ. Modell. Software*, **75**, 273–316, https://doi.org/10.1016/j.envsoft.2015.08.013.

——, C. J. F. Braak, H. V. Gupta, and B. A. Robinson, 2009: Equifinality of formal (DREAM) and informal (GLUE) Bayesian approaches in hydrologic modeling? *Stochastic Environ. Res. Risk Assess.*, **23**, 1011–1026, https://doi.org/10.1007/s00477-008-0274-y.

Vu, T. M., and A. K. Mishra, 2019: Nonstationary frequency analysis of the recent extreme precipitation events in the United States. *J. Hydrol.*, **575**, 999–1010, https://doi.org/10.1016/j.jhydrol.2019.05.090.

Wallemacq, P., T. Delbiso, R. Below, M. Wahlström, D. McClean, S. Landelle, B. Leoni, and R. House, 2015: The human cost of weather related disasters 1995-2015. United Nations Office for Disaster Risk Reduction Rep., 30 pp., https://reliefweb.int/sites/reliefweb.int/files/resources/COP21_WeatherDisastersReport_2015_FINAL.pdf.

Wang, J., and Coauthors, 2011: The Coupled Routing and Excess Storage (CREST) distributed hydrological model. *Hydrol. Sci. J.*, **56**, 84–98, https://doi.org/10.1080/02626667.2010.543087.

Watson, K. M., G. R. Harwell, D. S. Wallace, T. L. Welborn, V. G. Stengel, and J. S. McDowell, 2018: Characterization of peak streamflows and flood inundation of selected areas in southeastern Texas and southwestern Louisiana from the August and September 2017 flood resulting from Hurricane Harvey. U.S. Geological Survey Scientific Investigations Rep. 2018-5070, 56 pp., https://pubs.usgs.gov/sir/2018/5070/sir20185070.pdf.

Wing, O. E. J., P. D. Bates, C. C. Sampson, A. M. Smith, K. A. Johnson, and T. A. Erickson, 2017: Validation of a 30 m resolution flood hazard model of the conterminous United States. *Water Resour. Res.*, **53**, 7968–7986, https://doi.org/10.1002/2017WR020917.

——, C. C. Sampson, P. D. Bates, N. Quinn, A. M. Smith, and J. C. Neal, 2019: A flood inundation forecast of Hurricane Harvey using a continental-scale 2D hydrodynamic model. *J. Hydrol. X*, **4**, 100039, https://doi.org/10.1016/j.hydroa.2019.100039.

Wood, E. F., and Coauthors, 2011: Hyperresolution global land surface modeling: Meeting a grand challenge for monitoring Earth's terrestrial water: OPINION. *Water Resour. Res.*, **47**, W05301, https://doi.org/10.1029/2010WR010090.

Zhang, J., K. Howard, C. Langston, B. Kaney, Y. Qi, L. Tang, and H. Grams, 2016: Multi-Radar Multi-Sensor (MRMS) quantitative precipitation estimation: Initial operating capabilities. *Bull. Amer. Meteor. Soc.*, **97**, 621–638, https://doi.org/10.1175/BAMS-D-14-00174.1.

——, Y.-F. Huang, D. Munasinghe, Z. Fang, Y.-P. Tsang, and S. Cohen, 2018: Comparative analysis of inundation mapping approaches for the 2016 flood in the Brazos River, Texas. *J. Amer. Water Resour. Assoc.*, **54**, 820–833, https://doi.org/10.1111/1752-1688.12623.